Dominance of the phonon drag mechanism in the spin Seebeck effect at low temperatures

Roberto L. Rodríguez-Suárez[1] and Sergio M. Rezende[2,*]

[1]*Facultad de Física, Pontificia Universidad Católica de Chile, Casilla 306, Correo 22, Santiago, Chile*

[2]*Departamento de Física, Universidade Federal de Pernambuco, 50670-901 Recife, PE, Brazil*

(Received 10 August 2023; revised 19 September 2023; accepted 20 September 2023; published 6 October 2023)

The spin Seebeck effect (SSE) consists of the generation of a spin current in a magnetic insulator under a temperature gradient that is converted into a charge current in an attached thin metallic layer with strong spin-orbit interaction. The theoretical models proposed to explain the experimental observations of the SSE in the so-called longitudinal configuration consider that the spin current is entirely produced by the thermal excitation of magnons in the magnetic material. Here we show that actually, at low temperatures, the SSE is entirely dominated by a phonon drag mechanism, in which phonons in the heat current generate a spin current by means of magnon-phonon interaction. The theory explains quantitatively quite well the experimental observations of Iguchi *et al.* [Iguchi *et al.*, Phys. Rev. B **95**, 174401 (2017)], demonstrating that the SSE in yttrium iron garnet (YIG)/platinum structures has a pronounced peak at low temperatures following the behavior of the thermal conductivity in YIG.

DOI: 10.1103/PhysRevB.108.134407

I. INTRODUCTION

The spin Seebeck effect (SSE) consists of the generation of a spin current by a temperature gradient in a magnetic material, that is usually detected electrically by means of the inverse spin Hall effect in attached metallic contacts. Initially observed in a Permalloy film with a temperature gradient applied along the film, in the so-called transverse configuration [1], the SSE was subsequently demonstrated in the ferrimagnetic insulator $Y_3Fe_5O_{12}$ (yttrium iron garnet-YIG) in the same configuration [2]. Shortly after, the SSE was observed in a YIG slab with an attached platinum strip with the temperature difference applied across the bilayer structure, in the so-called longitudinal configuration [3], which became the standard structure to study the effect. Since then, intensive studies have been conducted on the SSE to investigate its detailed properties and elucidate the mechanisms involved in the generation of the spin currents [4–29], to observe the effect in other ferro- and ferrimagnetic materials [30–36], to investigate the effect and explain the mechanisms in antiferromagnetic insulators [37–50] and in paramagnets [51–55], and to develop thermoelectric applications [28,29,31], among others.

Most experiments for the study of the SSE have been performed using a junction made of a magnetic insulator and a paramagnetic metallic layer such as Pt, Pd, W, and Ta, that is used to convert the spin current generated by the thermal gradient into an electric current by means of the inverse spin Hall effect (ISHE). Since YIG/Pt enables driving and efficient electric detection of spin-current effects, the YIG/Pt junction is now recognized as a model system for SSE studies. Note that the theories proposed so far for the SSE in this and other systems are mainly based on the thermal generation of magnons at the interface of the junction or in the bulk of the magnetic layer, and despite the fact that there is mounting evidence that phonons may also play an important role in the SSE [56–61], insufficient effort has been made to present a full quantitative theory for the effect considering the direct participation of phonons. However, it is important to call attention to the fact that the strong enhancement of the SSE observed in the longitudinal configuration in $LaY_3Fe_5O_{12}$ at low temperatures was explained qualitatively in Ref. [56] by a phonon drag mechanism. That paper has served as an inspiration for the current work.

In this paper, we present a full quantitative theory for the SSE in a bilayer made of a ferro- or ferrimagnetic insulator (FMI) and a nonmagnetic metallic (NM) layer under a perpendicular temperature gradient. We show that the phonon current produced by the thermal gradient generates a magnonic spin current by means of a phonon drag mechanism mediated by the magnon-phonon interaction that, at low temperatures, is orders of magnitude larger than the pure magnonic current. The theory provides results for the temperature dependence of the SSE that are in quite good agreement with the experimental data of Iguchi *et al.* [60]. In Sec. II we review the basic properties of magnons, phonons, and the magnon-phonon interaction. Section III is devoted to a review of the theory for the pure bulk magnonic mechanism for the SSE. In Sec. IV, we develop the theory for the phonon drag contribution to the spin current and show that it explains quite well the experimentally measured temperature dependence of the SSE in gadolinium gallium garnet (GGG)/Pt/YIG/Pt devices. Finally, Sec. V is devoted to the conclusions.

II. MAGNONS, PHONONS, AND THEIR INTERACTION IN FERROMAGNETS

In a ferromagnetic insulator, the relevant elementary excitations are magnons and phonons, the quanta of, respectively, spin waves and elastic lattice vibrations. Actually, YIG is a

*Corresponding author: sergio.rezende@ufpe.br

ferrimagnet, but at low temperatures the magnetic properties are dominated by magnons in the acoustic branch that behave as ferromagnetic excitations. Here we present some basic properties of free magnons and phonons, and also of their interaction. We consider a ferromagnetic medium described by a Hamiltonian containing magnetic, elastic, and magnetoelastic contributions. The magnetic part consists of the interactions between individual spins $\vec{S}_i$ at site i with the magnetic field $\vec{H}$ (Zeeman interaction), and the exchange interaction between neighboring spins, that can be represented by the Hamiltonian [62–66]

$$\mathrm{H}_{\mathrm{mag}} = -g\mu_B \sum_i \vec{H}\cdot\vec{S}_i - 2J\sum_{i,\delta}\vec{S}_i\cdot\vec{S}_{i+\delta}, \tag{1}$$

where μ_B is the Bohr magneton, g is the spectroscopic splitting factor, and J is the nearest neighbor exchange interaction parameter between the spin $\vec{S}_i$ and its neighbor at $i+\delta$. Since the magnons involved in the SSE are away from the Brillouin zone center, we neglect the long-range dipolar interaction between the spins. We treat the quantized excitations of the magnetic system with the Holstein-Primakoff approach, which consists of transformations that express the components of the spin operator in terms of boson operators that create or destroy magnons [62–66].

In the first transformation, the components of the local spin operator are related to the creation and annihilation operators of spin deviation at site i, denoted, respectively, by $a_i^\dagger$ and a_i, which satisfy the boson commutation rules $[a_i, a_j^\dagger] = \delta_{ij}$ and $[a_i, a_j] = 0$. Using a coordinate system with $\hat{z}$ along the equilibrium direction of the spins, defining $S_i^+ = S_i^x + iS_i^y$ and $S_i^- = S_i^x - iS_i^y$, it can be shown that in first order the relations between the components of the spin operators and the operators of spin deviation are $S_i^+ \cong (2S)^{1/2}a_i$, $S_i^- \cong (2S)^{1/2}a_i^\dagger$, and $S_i^z = S - a_i^\dagger a_i$. The next step consists of introducing a transformation from the local field operators to collective boson operators by means of $a_i = N^{-1/2}\sum_k e^{i\vec{k}.\vec{r}_i}a_k$, where N is the number of spins in the system, $\vec{k}$ is the wave vector, and $a_k^\dagger$ and a_k are the creation and annihilation operators of magnons, which satisfy the boson commutation rules $[a_k, a_{k'}^\dagger] = \delta_{kk'}$ and $[a_k, a_{k'}] = 0$.

Using the transformations described in the spin Hamiltonian one can show that it can be written in a diagonal form representing noninteracting boson particles [62–66]

$$\mathrm{H}_m = \sum_k \hbar\omega_k a_k^\dagger a_k, \tag{2}$$

where ω_k is the frequency of magnons with wave vector $\vec{k}$. For YIG, it has been shown [66] that the dispersion relation in a spherical Brillouin zone is given by the approximate equation

$$\omega_k = \gamma H + \omega_{\mathrm{ZB}}\left(1 - \cos\frac{\pi k}{2k_m}\right), \tag{3}$$

where $\gamma = g\mu_B/\hbar$ is the gyromagnetic ratio, ω_{ZB} is the zone boundary frequency, and k_m is the value of the maximum wave number.

To treat the elastic system, we consider that the ferromagnetic crystal is a continuous solid, elastically isotropic, with average mass density ρ. We also assume that it is a cubic crystal so that, within the linear approximation, the relation between the stress tensor and the strain tensor involves only two different elastic constants, c_{12} and c_{44}. The elastic deformations of the solid are expressed in terms of the vector displacement $\vec{u} = \vec{r} - \vec{r}'$, where $\vec{r}$ is the initial position of an atom or of a volume element, and $\vec{r}'$ is the position after deformation. The contributions of the elastic system to the Hamiltonian arise from the kinetic and potential energies. Introducing the momentum density conjugate to the displacement, $\rho\partial u_i/\partial t$, in the linear approximation, the elastic Hamiltonian can be written as [62–67]

$$\mathrm{H}_e = \int d^3r\left(\frac{\rho}{2}\frac{\partial u_i}{\partial t}\frac{\partial u_i}{\partial t} + \frac{\alpha}{2}\frac{\partial u_i}{\partial x_i}\frac{\partial u_j}{\partial x_j} + \frac{\beta}{2}\frac{\partial u_i}{\partial x_j}\frac{\partial u_i}{\partial x_j}\right), \tag{4}$$

where the elastic constants are written as $\alpha = c_{12} + c_{44}$, $\beta = c_{44}$, for a Cartesian coordinate system chosen with axes lying along the $\langle 100\rangle$ crystallographic directions. In order to obtain the collective excitation operators for the elastic system, we use the canonical transformation,

$$u_i(\vec{r},t) = \left(\frac{\hbar}{V}\right)^{1/2}\sum_{k,\mu}\varepsilon_{i\mu}(\vec{k})Q_k^\mu(t)e^{i\vec{k}\cdot\vec{r}}, \tag{5}$$

$$\rho\dot{u}_i(\vec{r},t) = \left(\frac{\hbar}{V}\right)^{1/2}\sum_{k,\mu}\varepsilon_{i\mu}(\vec{k})P_k^\mu(t)e^{-i\vec{k}\cdot\vec{r}}, \tag{6}$$

where $\varepsilon_{i\mu} = \hat{x}_i\cdot\hat{\varepsilon}(\vec{k},\mu)$ and $\hat{\varepsilon}(\vec{k},\mu)$ are unitary polarization vectors. We will denote by $\mu = 1, 2$ the two polarizations transverse to the wave vector $\vec{k}$, and $\mu = 3$ the longitudinal one. Notice that from Hermiticity it follows that $Q_k^\mu = Q_{-k}^{\mu+}$ and $P_k^\mu = P_{-k}^{\mu+}$. The quantization of the elastic vibrations is made through the commutation relations involving $u_i(\vec{r})$ and its conjugate momentum density $\rho\,\partial\vec{u}/\partial t$. The only noncommuting pair is such that $[u_i(\vec{r}), \rho\dot{u}_j(\vec{r}')] = i\hbar\delta_{ij}\delta(\vec{r}-\vec{r}')$, which leads to $[Q_k^\mu, P_{k'}^\nu] = i\hbar\delta_{kk'}\delta_{\mu\nu}$.

In order to diagonalize the elastic Hamiltonian it is necessary to introduce the canonical transformations,

$$Q_k^\mu = \left[\frac{\hbar}{2\rho\omega_{p\mu}(k)}\right]^{1/2}(b_{\mu-k}^\dagger + b_{\mu k}), \tag{7}$$

$$P_k^\mu = i\left[\frac{\rho\hbar\omega_{p\mu}(k)}{2}\right]^{1/2}(b_{\mu k}^\dagger - b_{\mu-k}), \tag{8}$$

where the new operators satisfy the boson commutation relations $[b_{\mu k}, b_{\nu k'}] = 0$, $[b_{\mu k}, b_{\nu k'}^\dagger] = \delta_{\mu\nu}\delta_{kk'}$, and are interpreted as creation and annihilation operators of lattice vibrations, whose quanta are the phonons, and

$$\omega_{p\mu}(k) = k[(\beta + \alpha\delta_{\mu 3})/\rho]^{1/2} \tag{9}$$

is the frequency of phonons with wave number k and polarization μ. With transformations (5)–(8), the Hamiltonian in Eq. (4) becomes

$$\mathrm{H}_e = \sum_{k,\mu}\hbar\omega_{p\mu}(k)(b_{\mu k}^\dagger b_{\mu k} + 1/2), \tag{10}$$

which represents a system of noninteracting bosons. In terms of the operators in Eqs. (7) and (8), the displacement and the momentum density operators become

$$u_i = \left(\frac{\hbar}{2\rho V}\right)^{1/2} \sum_{k,\mu} \varepsilon_{i\mu}(\vec{k})\omega_{p\mu}^{-1/2}(b_{\mu k}^{\dagger} e^{-i\vec{k}\cdot\vec{r}} + b_{\mu k} e^{i\vec{k}\cdot\vec{r}}), \quad (11)$$

$$\rho\dot{u}_i = \left(\frac{\rho\hbar}{2V}\right)^{1/2} \sum_{k,\mu} i\varepsilon_{i\mu}(\vec{k})\omega_{p\mu}^{1/2}(b_{\mu k}^{\dagger} e^{i\vec{k}\cdot\vec{r}} - b_{\mu k} e^{-i\vec{k}\cdot\vec{r}}). \quad (12)$$

Due to the spin-orbit interaction, the elastic displacements in a magnetic medium are coupled to the spin excitations. This is what ultimately relaxes the magnetization dynamics in any magnetic material, gives rise to the magnetostrictive properties, and also produces the coupling between spin and elastic waves.

Note that if a spin wave and an elastic wave have frequency and wave vector close to each other, they become strongly coupled giving rise to hybrid excitations, called magnetoelastic waves, or magnon-phonon hybrid excitations [62–67]. Magnetoelastic waves with frequency in the microwave region were first observed experimentally in 1963 in YIG [68] and soon attracted interest for the study of their properties and possible applications in microwave devices [68–71]. In recent years they gained renewed interest with the advent of the field of spintronics [72–88]. Since in a fixed magnetic field the crossing of the magnon and phonon dispersion relations occupies a very small region in the Brillouin zone, the influence of magnetoelastic waves in the spin Seebeck effect is quite small and is relevant only in a few experiments [59]. For this reason, we do not explore here the detailed properties of the magnetoelastic wave. Instead, as we shall show, the phonon drag process that dominates the SSE at low temperatures relies on one-phonon–two-magnon interaction.

The magnetoelastic interaction can be expressed by a phenomenological Hamiltonian, which is a function of the spin $\vec{S}$ and the displacement $\vec{u}$. For a cubic crystal, with the static field applied along one of the [100] directions, the lowest-order term of the interaction Hamiltonian is given by [62–67]

$$\mathrm{H_{me}} = \int d^3r \frac{b_1}{S^2}\left(S_x^2\, e_{xx} + S_y^2\, e_{yy} + S_z^2\, e_{zz}\right) + \frac{2b_2}{S^2}\left(S_x S_y e_{xy} + S_y S_z e_{yz} + S_z S_x e_{zx}\right), \quad (13)$$

where

$$e_{ij} = \frac{1}{2}\left(\frac{\partial u_i}{\partial x_j} + \frac{\partial u_j}{\partial x_i}\right) \quad (14)$$

is the strain, and b_1 and b_2 are the magnetoelastic interaction constants. Considering the magnetic field applied in the FMI film plane in the z direction and the temperature gradient applied in the y direction, the phonons in the thermal current have a wave vector in the y direction, so that only strain components with $\partial u_i/\partial y$ are nonzero. Thus the only terms in the magnetoelastic that contribute to the one-phonon—two-magnon interaction is

$$\mathrm{H_{me}} = \int d^3r \left[\frac{b_1}{2S^2}\left(S_y^2 \frac{\partial u_y}{\partial y}\right) + \frac{b_2}{S^2}\left(S_x S_y \frac{\partial u_x}{\partial y}\right)\right]. \quad (15)$$

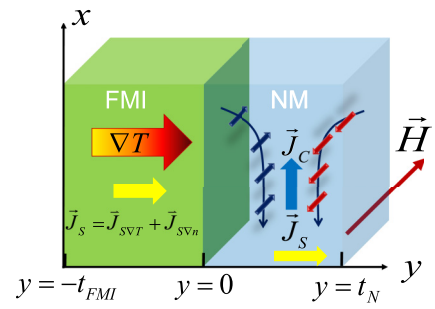

FIG. 1. Illustration of the ferromagnetic insulator (FMI)/normal metal (NM) bilayer and coordinate axes used to formulate the theoretical model for the generation of spin current by the temperature gradient in the spin Seebeck effect.

The first term in this equation contains the contribution from longitudinal phonons, while the second one is due to transverse phonons. Using the transformations from the spin operators into magnon creation and annihilation operators, one can show that the second term only leads to the creation or annihilation of two magnons, which are not of interest here. Considering only the first term in Eq. (15), corresponding to longitudinal phonons, the Hamiltonian for one-phonon–two-magnon interaction gives, after the transformations from the spin and displacement operators into magnon and phonon operators,

$$\mathrm{H}_{m-p} = \sum_{k_1,k,q} (V_{m-p} b_{qp} a_{k_1} a_k^{\dagger} + V_{m-p}^{*} b_{qp}^{\dagger} a_{k1}^{\dagger} a_k)\Delta(\vec{k}_1 + \vec{q}_p - \vec{k}), \quad (16)$$

where

$$V_{m-p} = \frac{b_1}{4SN}\left(\frac{\hbar V}{2\rho}\right)^{1/2} q_p \omega_{qp}^{-1/2}. \quad (17)$$

The Hamiltonian (16) represents a process in which a magnon with wave vector $\vec{k}_1$ (in thermal equilibrium) interacts with a phonon of wave vector $\vec{q}_p$ in the thermal bath to generate another magnon $\vec{k}$ by a three-boson process that conserves momentum and energy. As we shall show in Sec. IV, this is the process responsible for the generation of a spin current mediated by phonons.

III. MAGNONIC THEORY FOR THE SPIN SEEBECK EFFECT IN FERROMAGNETIC INSULATORS

In this section we review the theory for the spin Seebeck effect considering only the spin current transported by magnons in a FMI in contact with a NM layer, under a temperature gradient normal to the plane and with a static magnetic field H applied in the plane, as illustrated in Fig. 1. We assume that the FMI has one spin per unit cell, so that there is only one magnon mode. Note that we consider only the bulk magnon theory [13,19,44] because it has been shown [89] that in YIG/Pt, at room temperature, this mechanism completely dominates the SSE in YIG films with thickness larger than 100 nm.

Our goal here is to calculate the spin current created by the thermal gradient in the FMI and injected into the NM layer. The spin current flows into and diffuses in the NM

layer where it is partially converted into a transverse charge current by the ISHE [90–92] producing a DC voltage that is a signature of the SSE. The magnon spin current due to the thermal gradient across the thickness can be calculated with Boltzmann and diffusion equations imposing the appropriate boundary conditions. We choose a coordinate system with the z axis parallel to the magnetic field H applied in the easy plane along the easy axis of the bilayer, and the y axis perpendicular to the plane, as in Fig. 1.

Considering z the equilibrium direction of the spins, the spin-current density with polarization z carried by magnons with wave vector $\vec{k}$ and energy $\varepsilon_k = \hbar\omega_k$ is [7,8,13,19,44]

$$\vec{J}_S^z = \frac{\hbar}{(2\pi)^3}\int d^3k\vec{v}_k\big[n_k(\vec{r}) - n_k^0\big], \tag{18}$$

where $\vec{v}_k$ is the magnon velocity, $n_k(\vec{r})$ is the number of magnons with wave vector $\vec{k}$ at a position $\vec{r}$, and n_k^0 is the number in thermal equilibrium, given by the Bose-Einstein distribution with zero chemical potential $n_k^0(\varepsilon_k) = [e^{\varepsilon_k/k_BT} - 1]^{-1}$. We consider that the temperature T of the magnon system is the same as that of the lattice, since there is no experimental evidence that they are significantly different [12,93]. Under the influence of external perturbations, such as thermal gradients, the magnon number $n_k(\vec{r})$ becomes nonuniform, and its distribution can be calculated with the Boltzmann transport and the diffusion equations subject to the boundary conditions. One approach to this problem consists of using the concept of magnon accumulation $\delta n_m(\vec{r})$, introduced by Zhang and Zhang [7,8], defined as the density of magnons in excess of equilibrium,

$$\delta n_m(\vec{r}) = \frac{1}{(2\pi)^3}\int d^3k\big[n_k(\varepsilon_k,\vec{r}) - n_k^0\big], \tag{19}$$

and finding the evolution of $\delta n_m(\vec{r})$. The distribution of the magnon number under the influence of a thermal gradient can be calculated with the Boltzmann transport equation. In the absence of external forces and in the relaxation approximation, in steady state the Boltzmann equation gives [13,19,44,66]

$$n_k(\vec{r}) - n_k^0 = -\tau_k\vec{v}_k\cdot\nabla n_k(\vec{r}), \tag{20}$$

where τ_k is the k-magnon relaxation time. In the spirit of linear response theory, we write the excess magnon number as the sum of the equilibrium distribution plus a small deviation in the form [94]

$$n_k(\vec{r}) = n_k^0 + n_k^0\lambda_k g(\vec{r}), \tag{21}$$

where $g(\vec{r})$ is a spatial distribution to be determined by the solution of the boundary value problem and $\lambda_k(\varepsilon_k)$ is a function of the magnon energy. Following [19], we use an expansion for $\lambda_k(\varepsilon_k)$ that in lowest order of energy is chosen to eliminate the singularity at $\varepsilon_k = 0$, namely,

$$n_k(\vec{r}) = n_k^0 + n_k^0\varepsilon_k g(\vec{r}). \tag{22}$$

Using Eqs. (20) and (22) in Eq. (18), one obtains a magnonic spin current with two components, $\vec{J}^z_{S\nabla T}$ due to the thermal gradient, and $\vec{J}^z_{S\nabla n}$ due to the spatial gradient. The total spin-current density is [19]

$$\vec{J}_S^z = -S_S^z\nabla T - \hbar D_m\nabla\delta n_m(\vec{r}), \tag{23}$$

where

$$S_S^z = \frac{\hbar}{(2\pi)^3 T}\int d^3k\tau_k v_{ky}^2\frac{e^x x}{(e^x-1)^2}, \tag{24}$$

where T is the average temperature, $x = \varepsilon_k/k_BT$ is the normalized magnon energy, the integral is evaluated over the first Brillouin zone,

$$D_m = \frac{1}{(2\pi)^3 I_0}\int d^3\, k\tau_k\, v_{ky}^2\, n_k^0\varepsilon_k \tag{25}$$

is the magnon diffusion coefficient, and

$$I_0 = \frac{1}{(2\pi)^3}\int d^3k n_k^0\varepsilon_k. \tag{26}$$

As shown in Ref. [44], the magnon accumulation is proportional to the magnon chemical potential $\mu_m(\vec{r})$, used to characterize the nonequilibrium magnon Bose-Einstein distribution. This explains why Eq. (23) is the same as the one obtained in the formulation of the theory for the SSE in terms of the magnon chemical potential [21].

Considering that the magnon accumulation relaxes into the lattice with a magnon-phonon relaxation time $\tau_{\rm mp}$, conservation of angular momentum implies that $\nabla\cdot\vec{J}^z_{S\nabla n_m} = -\hbar\delta n_m/\tau_{\rm mp}$. Using this relation in Eq. (23) leads to a diffusion equation for the magnon accumulation,

$$\nabla^2\delta n_m = \frac{\delta n_m}{l_m^2}, \tag{27}$$

where $l_m = (D_m\tau_{\rm mp})^{1/2}$ is the magnon diffusion length. Considering the spatial variation only in the y direction, solution of Eq. (27) gives, for the magnon accumulation,

$$\delta n_m(y) = A\cosh[(y+t_{\rm FMI})/l_m] + B\sinh[(y+t_{\rm FMI})/l_m], \tag{28}$$

and the corresponding spin-current density calculated with Eq. (23) is

$$J_{\nabla n}(y) = -\frac{\hbar D_m}{l_m}\{A\sinh[(y+t_{\rm FMI})/l_m] + B\cosh[(y+t_{\rm FMI})/l_m]\}. \tag{29}$$

Thus the total spin-current density in the FMI ($-t_{\rm FMI}\leqslant y\leqslant 0$) is

$$J_S(y) = -S_S\nabla_y T - \frac{\hbar D_m}{l_m}A\sinh[(y+t_{\rm FMI})/l_m] - \frac{\hbar D_m}{l_m}B\cosh[(y+t_{\rm FMI})/l_m], \tag{30}$$

where the coefficients A and B are obtained imposing the boundary conditions at $y = -t_{\rm FMI}$ and $y = 0$, determined by conservation of the angular momentum flow that requires continuity of the spin currents at the interfaces. As shown in Refs. [19,44], the precessing spins associated with the magnon accumulation at the FMI/NM interface inject a spin current into the NM layer by the spin-pumping process given by

$$J_S(0^+) = -C_S\nabla_y T, \tag{31}$$

where the coefficients are

$$C_S = b\frac{S_S l_m}{\hbar D_m}\rho g_{\rm eff}^{\uparrow\downarrow}, \tag{32}$$

$$b = \frac{\gamma\hbar}{2\pi M I_0}\frac{1}{(2\pi)^3}\int d^3k n_k^0 \varepsilon_k^2, \tag{33}$$

while $g_{\rm eff}^{\uparrow\downarrow}$ is the effective spin-mixing conductance, that takes into account the spin-pumped and back-flow spin currents [95], and

$$\rho = \frac{\cosh(t_{\rm FMI}/l_m) - 1}{\sinh(t_{\rm FMI}/l_m)} \tag{34}$$

is a thickness factor, such that $\rho \approx 1$ for $t_{\rm FMI} \gg l_m$ and $\rho \approx 0$ for $t_{\rm FMI} \ll l_m$.

Equations (31) and (32) show that the magnonic spin current at the FMI/NM interface generated by a thermal gradient perpendicular to the bilayer plane is proportional to the temperature gradient and to the spin-mixing conductance of the interface. The spin current $\vec{J}_S$ flowing into the NM layer diffuses with diffusion length λ_N, and generates a charge current density $\vec{J}_C = \theta_{\rm SH}(2e/\hbar)\vec{J}_S \times \hat{\sigma}$ by the ISHE [90–92] that produces a SSE voltage at the ends of the NM layer. The voltage at the ends of the NM layer is obtained by integrating the charge current density along x and y and is given by [13,19,44]

$$V_{\rm SSE} = R_N w \lambda_N \frac{2e}{\hbar}\theta_{\rm SH}\tanh\left(\frac{t_N}{2\lambda_N}\right) J_S(0), \tag{35}$$

where R_N, t_N and w are, respectively, the resistance, thickness, and width of the NM layer and $J_S(0)$ is given by Eqs. (31)–(34).

The spin Seebeck coefficient is often defined with reference to the voltage measured in the NM. One disadvantage of this definition is that the voltage varies with the resistance, so that two samples made with the same material but with different NM layer thicknesses have different spin Seebeck voltage coefficients. As in Ref. [44], we quantify the SSE by the current spin Seebeck coefficient, $S_{\rm SSE} = I_{\rm SSE}/\nabla_y T$, where $I_{\rm SSE} = V_{\rm SSE}/R_N$ is the charge current in the NM layer produced by the temperature gradient $\nabla_y T$. Thus, with Eqs. (31) and (35), we obtain

$$S_{\rm SSE} = w\lambda_N \frac{2e}{\hbar}\theta_{\rm SH}\tanh\left(\frac{t_N}{2\lambda_N}\right) C_S. \tag{36}$$

In order to compare the model for the SSE with experimental results for a specific FMI, one needs detailed information on the dispersion relations and relaxation rates for the magnon modes. They are used to calculate the integrals over the Brillouin zone that appear in the relevant parameters, such as the magnon drift parameter in Eq. (24), the diffusion coefficient in Eq. (25), and the spin-pumping parameter in Eq. (33).

Yttrium iron garnet is a ferrimagnet with 20 spins per unit cell, so it has a complicated magnon dispersion relation with one acoustic mode and 19 optical modes [96]. Since the lowest magnon optical branch lies above the zone-boundary value, the calculation of the thermal properties in the presence of an applied field H at temperatures up to 300 K can be done approximately considering only the acoustic branch, with a magnon dispersion given by [93]

$$\omega_k = \gamma H + \omega_{\rm ZB}\left(1 - \cos\frac{\pi k}{2k_m}\right), \tag{37}$$

where $\gamma = g\mu_B/\hbar$ is the gyromagnetic ratio, g is the spectroscopic splitting factor, μ_B the Bohr magneton, $\omega_{\rm ZB}$ the zone boundary frequency, and k_m is the value of the maximum wave number assuming a spherical Brillouin zone. Using the magnon group velocity obtained from Eq. (37), one can show [19,44] that the coefficient C_S in Eq. (32) becomes

$$C_S = F_{\rm FMI}\frac{B_1 B_S}{(B_0 B_2)^{1/2}}\rho g_{\rm eff}^{\uparrow\downarrow}, \tag{38}$$

where the factor $F_{\rm FMI}$ depends on material parameters and universal constants,

$$F_{\rm FMI} = \frac{\gamma\hbar k_B \tau_{mp}^{1/2}\tau_0^{1/2}k_m^2\omega_{\rm ZB}}{4\pi M\pi 2\sqrt{3}}, \tag{39}$$

and the parameters B in Eq. (38) are given by the integrals

$$B_S = \int_0^1 dq q^2 \sin^2\left(\frac{\pi q}{2}\right)\frac{e^x x}{\eta_q(e^x-1)^2},$$

$$B_1 = \int_0^1 dq q^2 \frac{x^2}{e^x - 1}, \tag{40}$$

$$B_0 = \int_0^1 dq q^2 \frac{x}{e^x - 1},$$

$$B_2 = \int_0^1 dq q^2 \sin^2\left(\frac{\pi q}{2}\right)\frac{x}{\eta_q(e^x-1)}. \tag{41}$$

In Eqs. (40) and (41) $q = k/k_m$ is a normalized wave number and $\eta_q = \eta_k/\eta_0$ is an adimensional relaxation rate, related to the magnon lifetime by $\eta_q = \tau_0/\tau_k$, where τ_0 is the lifetime of magnons near the zone center ($k \approx 0$). Following Refs. [13,19,44,66] we use for the magnon relaxation rate an expression obtained from fits to the calculated rates due to three- and four-magnon scattering processes,

$$\eta_q = 1.0 + (7.5\times 10^2 q)\left(\frac{T}{300}\right) + 10^3 \times (7.6q^2 - 4.9q^3)\left(\frac{T}{300}\right)^2, \tag{42}$$

where the relaxation time of the $k = 0$ mode was taken to be $\tau_0 = 1/\eta_0 = 5\times 10^{-8}$ s at $T = 300$ K. The magnon-phonon relaxation time $\tau_{\rm mp}$ that enters in Eq. (39) has been estimated in Refs. [13,19,44] to be $\tau_{\rm mp} \approx 10^{-12}$ s based on the value of the magnon diffusion length $l_m \approx 70$ nm obtained from the fit of Eq. (34) to the measured [18] thickness dependence of the SSE. Note that the value of the magnon diffusion length varies with the quality of the sample because it depends strongly on the magnon relaxation rate. Numerical evaluation of the integrals in Eqs. (40) and (41), using Eqs. (37) and (42), gives for 300 K the values $B_S = 2.0\times 10^{-4}$, $B_0 = 0.23$, $B_1 = 0.16$, and $B_2 = 6.9\times 10^{-5}$. Using these values, and the following parameters for YIG, $4\pi M = 1.76$ kG, $\gamma = 1.76\times 10^7$ s^{-1} Oe^{-1}, $H = 1$ kOe, $\omega_{\rm ZB}/2\pi = 7.0$ THz, and $k_m = 1.7\times 10^7$ cm^{-1}, considering $\rho = 1$ for $t_{\rm FMI} \gg l_m$ and the spin-mixing conductance for the YIG/Pt interface [18,19],

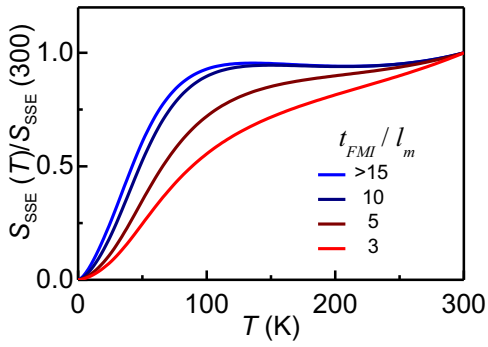

FIG. 2. (a) Calculated temperature dependence of the spin Seebeck coefficient in YIG/Pt for various YIG film thicknesses t_{FMI} relative to the magnon diffusion length l_m (300) at 300 K.

$g_{\text{eff}}^{\uparrow\downarrow} = 10^{14}\,\text{cm}^{-2}$, we obtain for the coefficient C_S in Eq. (38) $C_S = 2.9 \times 10^{-10}$ erg/(K cm). With this value and the parameters for the Pt layer, $\lambda_N = 3.7$ nm, $\theta_{\text{SH}} = 0.05$ [91,92], $w = 0.2$ cm, and $t_N = 4$ nm, we obtain the current spin Seebeck coefficient $S_{\text{SSE}} = I_{\text{SSE}}/\nabla_y T$, where $I_{\text{SSE}} = V_{\text{SSE}}/R_N$, for YIG/Pt at room temperature, $S_{\text{SSE}} = 0.17$ nA cm/K. Using this value, we find for the spin Seebeck voltage in YIG/Pt under a temperature gradient of $\nabla_y T = 200$ K/cm and a Pt layer with typical resistance $R_N = 200\,\Omega$, $V_{\text{SSE}} = 6.8\,\mu\text{V}$, which is in good quantitative agreement with values reported for YIG/Pt [13,97].

An important signature of a theoretical model for transport phenomena is the temperature dependence of physical quantities of interest. We have used Eqs. (36)–(42) to calculate the temperature dependence of the spin Seebeck coefficient in YIG/Pt under a magnetic field of $H = 1$ kOe to compare with experimental data. We neglect the variation with temperature of the spin-Hall angle θ_{SH} and the spin diffusion length λ_N of the Pt layer and consider for the magnon relaxation rate in YIG the dependence given in Eq. (42). Figure 2 shows the calculated temperature dependence of S_{SSE} for several YIG film thicknesses relative to the magnon diffusion relaxation rate decreases faster, so that the voltage increases. At low T the exponential decrease in the magnon population dominates so that the overall behavior exhibits the bump at ∼100 K, which is a characteristic feature of our model. This behavior is in good agreement with the experimental data reported in Ref. [13].

However, it turns out that, as recently realized, the experimental result for the temperature dependence of the SSE in Ref. [13] is incorrect. As pointed out in Ref. [60], the temperature difference ΔT across the YIG/GGG sample is smaller than the temperature difference ΔT_{set} measured by the two thermometers, because the temperature drop in intermediate layers introduced for any purpose can be very large at low temperatures. In the case of the experiments reported in Ref. [13], very thin GE-varnish layers were used to glue the YIG sample on the heat bath and on the Peltier module used to apply the temperature difference. Surprisingly, even though the thickness of each varnish layer is three orders of magnitude smaller than the one of the YIG/GGG sample, the fact that the thermal conductivity of the sample increases sharply at low temperatures results in the large drop in the ratio $\Delta T/\Delta T_{\text{set}}$. Thus, actually, the SSE at low temperatures, instead of following the behavior as in Ref. [13], has a sharp peak like the one reported in Ref. [60] for YIG. In the next section we show that at low temperatures, the dominant mechanism of the SSE is phonon drag, analogously to the conventional thermoelectric Seebeck effect in semiconductor silicon [98].

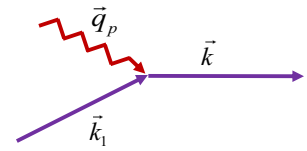

FIG. 3. Illustration of magnon-phonon interaction process by which phonons in the heat current generate a spin current.

IV. PHONON DRAG MECHANISM FOR THE SPIN SEEBECK EFFECT

As is well known, the thermal conductivity of insulators is orders of magnitude larger at low temperatures than at room temperature, and is dominated by the heat transport by phonons [99]. Thus phonons in the heat current can generate a spin current by means of the magnon-phonon interaction processes. We consider here the process illustrated in Fig. 3, in which a phonon with wave vector $\vec{q}_p$ in the heat current interacts with a magnon in thermal equilibrium with wave vector $\vec{k}_1$, to generate another magnon $\vec{k}$ by a three-boson process conserving momentum and energy.

The probability per unit time for the number of phonons n_q and the number of magnons n_{k1} to decrease by one unit, and the number of magnons n_k to increase by one unit in this process, calculated by Fermi's "golden rule" with Hamiltonian (16), is

$$W_{n_k \to n_k+1} = \frac{2\pi}{\hbar^2} \sum_{k_1} (V_{m-p})^2 [n_{k1} n_{qp} (n_k + 1)] \times \delta(\omega_{k1} + \omega_{qp} - \omega_k), \tag{43}$$

where V_{m-p} is given by Eq. (17) and the sum runs only over $\vec{k}_1$ because of the momentum conservation relation $\vec{k}_1 + \vec{q}_p = \vec{k}$. The reverse process by which the number of magnons $\vec{k}$ decreases by one unit is calculated in a similar manner, so that the time rate of change of the phonon number is given by

$$\frac{dn_k}{dt} = W_{n_k \to n_k+1} - W_{n_k \to n_k-1}. \tag{44}$$

Thus we find that the rate of change for the number of magnons in mode $\vec{k}$ to increase by means of the three-boson process is

$$\frac{dn_k}{dt} = \frac{2\pi}{\hbar^2} \sum_{k_1} (V_{m-p})^2 [n_{k1} n_{qp} (n_k + 1) - n_k (n_{k1} + 1)(n_{qp} + 1)] \delta(\omega_{k1} + \omega_{qp} - \omega_k). \tag{45}$$

In thermal equilibrium $dn_k/dt = 0$, so that we have the following relation for the thermal numbers:

$$\bar{n}_{k1}\bar{n}_{qp}(\bar{n}_k + 1) - (\bar{n}_{k1} + 1)(\bar{n}_{qp} + 1)\bar{n}_k = 0. \tag{46}$$

When there is a flow of heat or magnon current, the numbers of magnons and phonons are in excess of the thermal equilibrium numbers, so that following [99] we write

$$n_{k1} \to \bar{n}_{k1} + \delta n_{k1}, \quad n_k \to \bar{n}_k + \delta n_k, \quad n_{qp} \to \bar{n}_{qp} + \delta n_{qp}, \tag{47}$$

so that Eq. (45) becomes

$$\frac{dn_k}{dt} = \frac{2\pi}{\hbar^2}\sum_{k_1}(V_{m-p})^2[(\bar{n}_{k1} + \delta n_{k1})(\delta n_{qp} + \bar{n}_{qp})(\bar{n}_k + \delta n_k + 1) - (\bar{n}_k + \delta n_k)(\bar{n}_{k1} + \delta n_{k1} + 1)(\delta n_{qp} + \bar{n}_{qp} + 1)]\delta(\omega), \tag{48}$$

where $\delta(\omega)$ denotes conservation of energy. One can show that Eq. (48) gives

$$\frac{dn_k}{dt} = \frac{2\pi}{\hbar^2}\sum_{k_1}(V_{m-p})^2\left[-\frac{(\bar{n}_{k1}+1)}{(\bar{n}_k+1)}(\bar{n}_{qp}+1)\delta n_k + \frac{\bar{n}_k}{\bar{n}_{k1}}(\bar{n}_{qp}+1)\delta n_{k1} + (\bar{n}_{k1}+1)\frac{\bar{n}_k}{\bar{n}_{qp}}\right]\delta(\omega). \tag{49}$$

Now, since the magnon-phonon interaction is small, we consider that the number of phonons in excess of equilibrium is much larger than the perturbations in the magnon system, so in Eq. (43) we neglect δn_{k_1} and δn_k in the presence of n_{qp}. Also, considering energy and momentum conservation, and replacing the sum by an integral over the Brillouin zone in the usual way, one can show that at low temperatures Eq. (49) leads, approximately, to

$$\frac{dn_k}{dt} = F_{qp}\delta n_{qp}, \tag{50}$$

where

$$F_{qp} = \frac{\gamma b_1^2 q_q^2}{32MS\rho\omega_{qp}}\frac{a^3}{(2\pi)^2} \times \int d^3\, k_1(\bar{n}_{k1}+1)\frac{\bar{n}_{k1+qp}}{\bar{n}_{qp}}\delta(\omega_{k1} + \omega_{qp} - \omega_{k1+qp}). \tag{51}$$

Using this result in the time-dependent Boltzmann equation without external forces [98], we obtain

$$F_{qp}\delta n_{qp} = \frac{\partial n_k(\vec{r})}{\partial t} + \vec{v}_k \cdot \nabla_r n_k(\vec{r}) + \frac{n_k(\vec{r}) - n_k^0}{\tau_k}. \tag{52}$$

In steady state and considering only the phonon contribution to the magnon spin current, we have

$$n_k(\vec{r}) - n_k^0 = F_{qp}\delta n_{qp}\tau_k. \tag{53}$$

Using this result in Eq. (18), we obtain, for the phonon drag magnonic spin-current density,

$$\vec{J}_S^z(y) = \hat{y}\frac{\hbar}{(2\pi)^3}\int d^3k v_{ky}F_{qp}\delta n_{qp}\tau_k. \tag{54}$$

The goal now is to relate the phonon drag spin current to the phonon thermal current,

$$\vec{J}_Q = \frac{1}{V}\sum_{\vec{q}_p} f(\vec{q}_p, \vec{r})\varepsilon_{qp}\vec{v}_{qp}, \tag{55}$$

where $f(\vec{q}_p, \vec{r})$ is the phonon distribution function. From this equation one derives [99] the well-known relation

$$\vec{J}_Q = -K_{\rm th}\nabla T, \tag{56}$$

where $K_{\rm th}$ is the thermal conductivity. It can be shown that, at low temperatures, the phonon thermal current is dominated by phonons in a small width Δq_p in wave vector space, centered in a wave number q_p around $2 \times 10^7\ {\rm cm}^{-1}$. Thus the phonon current can be written approximately as

$$J_Q \approx G_{qp}\delta n_{qp}, \tag{57}$$

where

$$G_q = \frac{1}{2\pi^2}q_{qp}^3\Delta q_p\hbar v_{qp}^2. \tag{58}$$

Thus, with the relation (56), we have

$$\delta n_{qp} = -\frac{K_{\rm th}}{G_{qp}}\nabla T. \tag{59}$$

So, finally, the phonon drag spin current in Eq. (54) can be written as

$$\vec{J}_S(y) = -B\frac{F_q}{G_{qp}}K_{\rm th}\nabla T, \tag{60}$$

where

$$B = \frac{\hbar}{(2\pi)^3}\int d^3k v_{ky}\tau_k. \tag{61}$$

Equation (60) shows that the spin current produced by the phonon drag is proportional to the thermal conductivity, as revealed by the measurements of Iguchi *et al.* [60]. It also shows that the phonon drag contribution vanishes if the magnetoelastic interaction b_1 is null, as expected. Using for YIG the magnon dispersion relation (37), the parameter B in Eq. (61) becomes

$$B = \frac{\hbar}{4\pi}\frac{\omega_{\rm ZB}k_{\rm max}^2}{\eta_0}B_\eta, \tag{62}$$

where the coefficient

$$B_\eta = \int_0^1 \frac{\sin(\pi q/2)}{\eta_q(T)}q^2 dq \tag{63}$$

is written in terms of dimensionless variables to be evaluated numerically using the magnon relaxation rate in Eq. (42). For the evaluation of the parameter F_{qp}, we use a well-known expression for the δ function to write the integral in Eq. (51)

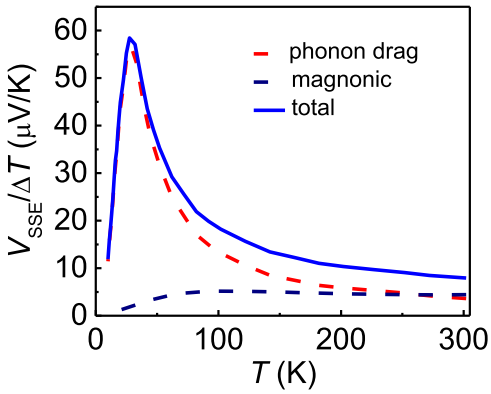

FIG. 4. Contributions of the calculated temperature dependence of the SSE voltage in YIG/Pt by the pure magnonic spin current (dashed dark blue curve), phonon drag spin current (dashed red curve), and the sum of the two (blue curve).

as

$$\int d^3\, k_1 f(k_1)\delta[g(k_1)] = \sum_i \frac{f(k_{1(i)})}{|g'(k_{1(i)})|}, \tag{64}$$

where $g'(k_{1(i)})$ denotes the derivative of the function $g(k_1)$ relative to k_1 calculated at the root (i) of $g(k_1) = 0$. With the magnon dispersion relation in Eq. (37), and with the phonon dispersion $\omega_{qp} = v_{qp}\, q_p$, the numerical calculation gives only one root in the first Brillouin zone, so that

$$g'(k_1) = \frac{\pi\omega_{\rm ZB}}{2k_m}\left[\sin\frac{\pi k_1}{2k_m} - \sin\frac{\pi(q_p + k_1)}{2k_m}\right]. \tag{65}$$

The phonon drag spin current as a function of temperature is calculated with Eq. (60), using the integrals (63) and (64) evaluated numerically and the experimentally measured thermal conductivity for YIG reported by Iguchi *et al.* [60]. Since $K_{\rm th}$ is measured at discrete temperatures from 10 to 300 K, the integrals are calculated for the same temperatures of the data, using the parameters for YIG given at the end of Sec. III and $\rho = 5.2\,{\rm g/cm^3}$, $v_{pq} = 7.21\times10^5$ cm/s (LA phonons), and $b_1 = 3.5\times10^6\,{\rm erg/cm^3}$. The values of Δq_p, q_p, and η_0 are adjusted so that the peak value of the spin Seebeck voltage $V_{\rm SSE}$ agrees with the one measured by Iguchi *et al.* [60]. The contributions to $V_{\rm SSE}/\Delta T$ from the pure magnonic spin current, from the phonon drag spin current and the sum of them are shown in Fig. 4. The pure magnonic contribution is calculated as in Sec. III using the value at $T = 300$ K as measured in [60] without the correction in the temperature difference. The sum of the magnonic and phonon drag spin contributions is in very good agreement with the data reported in [60]. Clearly, the phonon drag mechanism completely dominates the SSE at low temperatures, where its contribution is over two orders of magnitude larger than the magnonic contribution.

V. CONCLUSIONS

In summary, we have presented a full theory for the spin Seebeck effect in a FMI/NM bilayer under a thermal gradient applied perpendicularly to the bilayer plane. We have shown that the SSE voltage is made of two contributions, one due to the pure magnonic spin current excited in the bulk of the FMI layer by the thermal gradient, and another due to the spin current generated by the phonon drag mechanism. At room temperature the magnonic contribution is very important. However, at low temperatures, the SSE is completely dominated by a phonon drag mechanism, in which phonons in the heat current generate a spin current by means of the magnon-phonon interaction. The theory explains very well the experimental observations of Iguchi *et al.* [60], demonstrating that the SSE in yttrium iron garnet (YIG)/platinum structures has a pronounced peak at low temperatures following the behavior of the thermal conductivity in YIG.

ACKNOWLEDGMENTS

This research was supported in Brazil by Conselho Nacional de Desenvolvimento Científico e Tecnológico (CNPq), Coordenação de Aperfeiçoamento de Pessoal de Nível Superior (CAPES), Financiadora de Estudos e Projetos (FINEP), and Fundação de Amparo à Ciência e Tecnologia do Estado de Pernambuco (FACEPE), and in Chile by Fondo Nacional de Desarrollo Científico y Tecnológico (FONDECYT), Grant No. 1210641. S.M.R. acknowledges support of the INCT of Spintronics and Advanced Magnetic Nanostructures (INCT-SpinNanoMag), CNPq Grant No. 406836/2022–1.

[1] K. Uchida, S. Takahashi, K. Harii, J. Ieda, W. Koshibae, K. Ando, S. Maekawa, and E. Saitoh, Observation of spin Seebeck effect, Nature (London) **455**, 778 (2008).

[2] K. Uchida, J. Xiao, H. Adachi, J. Ohe, S. Takahashi, J. Ieda, T. Ota, Y. Kajiwara, H. Umezawa, H. Kawai, G. E. W. Bauer, S. Maekawa, and E. Saitoh, Spin Seebeck insulator, Nat. Mater. **9**, 894 (2010).

[3] K. Uchida, H. Adachi, T. Ota, H. Nakayama, S. Maekawa, and E. Saitoh, Observation of longitudinal spin-Seebeck effect in magnetic insulators, Appl. Phys. Lett. **97**, 172505 (2010).

[4] J. Xiao, G. E. W. Bauer, K.-c. Uchida, E. Saitoh, and S. Maekawa, Theory of magnon-driven spin Seebeck effect, Phys. Rev. B **81**, 214418 (2010).

[5] H. Adachi, J.-i. Ohe, S. Takahashi, and S. Maekawa, Linear-response theory of spin Seebeck effect in ferromagnetic insulators, Phys. Rev. B **83**, 094410 (2011).

[6] G. E. W. Bauer, E. Saitoh, and B. J. van Wees, Spin caloritronics, Nat. Mater. **11**, 391 (2012).

[7] Steven S.-L. Zhang and S. Zhang, Magnon mediated electric current drag across a ferromagnetic insulator layer, Phys. Rev. Lett. **109**, 096603 (2012).

[8] Steven S.-L. Zhang and S. Zhang, Spin convertance at magnetic interfaces, Phys. Rev. B **86**, 214424 (2012).

[9] S. Hoffman, K. Sato, and Y. Tserkovnyak, Landau-Lifshitz theory of the longitudinal spin Seebeck effect, Phys. Rev. B **88**, 064408 (2013).

[10] L. Chotorlishvili, Z. Toklikishvili, V. K. Dugaev, J. Barnás, S. Trimper, and J. Berakdar, Fokker-Planck approach to the theory of the magnon-driven spin Seebeck effect, Phys. Rev. B **88**, 144429 (2013).

[11] M. Schreier, A. Kamra, M. Weiler, J. Xiao, G. E. W. Bauer, R. Gross, and S. T. B. Goennenwein, Magnon, phonon, and electron temperature profiles and the spin Seebeck effect in magnetic insulator/normal metal hybrid structures, Phys. Rev. B **88**, 094410 (2013).

[12] M. Agrawal, V. I. Vasyuchka, A. A. Serga, A. D. Karenowska, G. A. Melkov, and B. Hillebrands, Direct measurement of magnon temperature: New insight into magnon-phonon coupling in magnetic insulators, Phys. Rev. Lett. **111**, 107204 (2013).

[13] S. M. Rezende, R. L. Rodríguez-Suárez, R. O. Cunha, A. R. Rodrigues, F. L. A. Machado, G. A. Fonseca Guerra, J. C. López Ortiz, and A. Azevedo, Magnon spin-current theory for the longitudinal spin-Seebeck effect, Phys. Rev. B **89**, 014416 (2014).

[14] K. Uchida, M. Ishida, T. Kikkawa, A. Kirihara, T. Murakami, and E. Saitoh, Longitudinal spin Seebeck effect: From fundamentals to applications, J. Phys.: Condens. Matter **26**, 343202 (2014).

[15] S. R. Boona, R. C. Myers, and J. P. Heremans, Spin caloritronics, Energy Environ. Sci. **7**, 885 (2014).

[16] U. Ritzmann, D. Hinzke, and U. Nowak, Propagation of thermally induced magnonic spin currents, Phys. Rev. B **89**, 024409 (2014).

[17] T. Kikkawa, K.-i. Uchida, S. Daimon, Z. Qiu, Y. Shiomi, and E. Saitoh, Critical suppression of spin Seebeck effect by magnetic fields, Phys. Rev. B **92**, 064413 (2015).

[18] A. Kehlberger, U. Ritzmann, D. Hinzke, E.-J. Guo, J. Kramer, G. Jakob, M. C. Onbasli, D. H. Kim, C. A. Ross, M. B. Jungfleisch, B. Hillebrands, U. Nowak, and M. Kläui, Length scale of the spin Seebeck effect, Phys. Rev. Lett. **115**, 096602 (2015).

[19] S. M. Rezende, R. L. Rodríguez-Suárez, J. C. López Ortiz, and A. Azevedo, Bulk magnon spin current theory for the longitudinal spin Seebeck effect, J. Magn. Magn. Mater. **400**, 171 (2016).

[20] V. Basso, E. Ferraro, A. Magni, A. Sola, M. Kuepferling, and M. Pasquale, Nonequilibrium thermodynamics of the spin Seebeck and spin Peltier effects, Phys. Rev. B **93**, 184421 (2016).

[21] L. J. Cornelissen, K. J. H. Peters, G. E. W. Bauer, R. A. Duine, and B. J. van Wees, Magnon spin transport driven by the magnon chemical potential in a magnetic insulator, Phys. Rev. B **94**, 014412 (2016).

[22] H. Yu, S. D. Brechet, and J.-P. Ansermet, Spin caloritronics, origin and outlook, Phys. Lett. A **381**, 825 (2017).

[23] A. Prakash, B. Flebus, J. Brangham, F. Yang, Y. Tserkovnyak, and J. P. Heremans, Evidence for the role of the magnon energy relaxation length in the spin Seebeck effect, Phys. Rev. B **97**, 020408(R) (2018).

[24] J. S. Jamison, Z. Yang, B. L. Giles, J. T. Brangham, G. Wu, P. Chris Hammel, F. Yang, and R. C. Myers, Long lifetime of thermally excited magnons in bulk yttrium iron garnet, Phys. Rev. B **100**, 134402 (2019).

[25] B. Flebus, Y. Tserkovnyak, and G. A. Fiete, Interfacial spin Seebeck effect in noncollinear magnetic systems, Phys. Rev. B **99**, 224410 (2019).

[26] S. S. Costa and L. C. Sampaio, Recent progress in the spin Seebeck and spin Peltier effects in insulating magnets, J. Magn. Magn. Mater. **547**, 168773 (2020).

[27] K.-I. Uchida, Spin caloritronics, in *Materials Science and Materials Engineering* (Elsevier, Amsterdam, 2022).

[28] S. Maekawa, T. Kikkawa, H. Chudo, J.-I. Ieda, and E. Saitoh, Spin and spin current—from fundamentals to recent progress, J. Appl. Phys. **133**, 020902 (2023).

[29] T. Kikkawa and E. Saitoh, Spin seebeck effect: sensitive probe for elementary excitation, spin correlation, transport, magnetic order, and domains in solids, Annu. Rev. Condens. Matter Phys. **14**, 129 (2023).

[30] C. M. Jaworski, J. Yang, S. Mack, D. D. Awschalom, R. C. Myers, and J. P. Heremans, Observation of the spin-Seebeck effect in a ferromagnetic semiconductor, Nat. Mater. **9**, 898 (2010).

[31] K. Uchida, H. Adachi, T. Kikkawa, A. Kirihara, M. Ishida, S. Yorozu, S. Maekawa, and E. Saitoh, Thermoelectric generation based on spin Seebeck effects, Proc. IEEE **104**, 1946 (2016).

[32] N. Ito, T. Kikkawa, J. Barker, D. Hirobe, Y. Shiomi, and E. Saitoh, Spin Seebeck effect in the layered ferromagnetic insulators $CrSiTe_3$ and $CrGeTe_3$, Phys. Rev. B **100**, 060402(R) (2019).

[33] Z. Li, J. Krieft, A. V. Singh, S. Regmi, A. Rastogi, A. Srivastava, Z. Galazka, T. Mewes, A. Gupta, and T. Kuschel, Vectorial observation of the spin Seebeck effect in epitaxial $NiFe_2O_4$ thin films with various magnetic anisotropy contributions, Appl. Phys. Lett. **114**, 232404 (2019).

[34] A. Akopyan, N. Prasai, B. A. Trump, G. G. Marcus, T. M. McQueen, and J. L. Cohn, Spin Seebeck effect in Cu_2OSeO_3: Test of bulk magnon spin current theory, Phys. Rev. B **101**, 100407(R) (2020).

[35] M. Elyasi and G. E. W. Bauer, Cryogenic spin Seebeck effect, Phys. Rev. B **103**, 054436 (2021).

[36] A. Anadon, E. Martin, S. Homkar, B. Meunier, M. Vergés, H. Damas, J. Alegre, C. Lefevre, F. Roulland, C. Dubs *et al.*, Thermal spin-current generation in the multifunctional ferrimagnet $Ga_{0.6}Fe_{1.4}O_3$, Phys. Rev. Appl. **18**, 054087 (2022).

[37] Y. Ohnuma, H. Adachi, E. Saitoh, and S. Maekawa, Spin Seebeck effect in antiferromagnets and compensated ferrimagnets, Phys. Rev. B **87**, 014423 (2013).

[38] S. Seki, T. Ideue, M. Kubota, Y. Kozuka, R. Takagi, M. Nakamura, Y. Kaneko, M. Kawasaki, and Y. Tokura, Thermal generation of spin current in an antiferromagnet, Phys. Rev. Lett. **115**, 266601 (2015).

[39] S. M. Wu, W. Zhang, A. KC, P. Borisov, J. E. Pearson, J. S. Jiang, D. Lederman, A. Hoffmann, and A. Bhattacharya, Antiferromagnetic spin Seebeck effect, Phys. Rev. Lett. **116**, 097204 (2016).

[40] S. M. Rezende, R. L. Rodríguez-Suárez, and A. Azevedo, Theory of the spin Seebeck effect in antiferromagnets, Phys. Rev. B **93**, 014425 (2016).

[41] A. Prakash, J. Brangham, F. Yang, and J. P. Heremans, Spin Seebeck effect through antiferromagnetic NiO, Phys. Rev. B **94**, 014427 (2016).

[42] Y. Shiomi, R. Takashima, D. Okuyama, G. Gitgeatpong, P. Piyawongwatthana, K. Matan, T. J. Sato, and E. Saitoh, Spin Seebeck effect in the polar antiferromagnet α-$Cu_2V_2O_7$, Phys. Rev. B **96**, 180414(R) (2017).

[43] J. Holanda, D. S. Maior, O. Alves Santos, L. H. Vilela-Leão, J. B. S. Mendes, A. Azevedo, R. L. Rodríguez-Suárez, and S. M. Rezende, Spin Seebeck effect in the antiferromagnet nickel oxide at room temperature, Appl. Phys. Lett. **111**, 172405 (2017).

[44] S. M. Rezende, R. L. Rodríguez-Suárez, and A. Azevedo, Magnon diffusion theory for the spin Seebeck effect in ferromagnetic and antiferromagnetic insulators, J. Phys. D: Appl. Phys. **51**, 174004 (2018).

[45] J. Li, Z. Shi, V. H. Ortiz, M. Aldosary, C. Chen, V. Aji, P. Wei, and J. Shi, Spin Seebeck effect from antiferromagnetic magnons and critical spin fluctuations in epitaxial FeF_2 films, Phys. Rev. Lett. **122**, 217204 (2019).

[46] P. R. T. Ribeiro, F. L. A. Machado, M. Gamino, A. Azevedo, and S. M. Rezende, Spin Seebeck effect in antiferromagnet nickel oxide in wide ranges of temperature and magnetic field, Phys. Rev. B **99**, 094432 (2019).

[47] W. Yuan, J. Li, and J. Shi, Spin current generation and detection in uniaxial antiferromagnetic insulators, Appl. Phys. Lett. **117**, 100501 (2020).

[48] D. Reitz, J. Li, W. Yuan, J. Shi, and Y. Tserkovnyak, Spin Seebeck effect near the antiferromagnetic spin-flop transition, Phys. Rev. B **102**, 020408(R) (2020).

[49] Y. Yamamoto, M. Ichioka, and H. Adachi, Antiferromagnetic spin Seebeck effect across the spin-flop transition: A stochastic Ginzburg-Landau simulation, Phys. Rev. B **105**, 104417 (2022).

[50] J. D. M. de Lima, P. R. T. Ribeiro, F. L. A. Machado, and S. M. Rezende, Enhanced spin Seebeck effect in the paramagnetic phase of the 3D Heisenberg antiferromagnet $RbMnF_3$, Phys. Rev. B **107**, L140406 (2023).

[51] S. M. Wu, J. E. Pearson, and A. Bhattacharya, Paramagnetic spin Seebeck effect, Phys. Rev. Lett. **114**, 186602 (2015).

[52] Y. Yamamoto, M. Ichioka, and H. Adachi, Spin Seebeck effect in paramagnets and antiferromagnets at elevated temperatures, Phys. Rev. B **100**, 064419 (2019).

[53] R. Luo, X. Zhao, L. Chen, T. J. Legvold, H. Navarro, I. K. Schuller, and D. Natelson, Spin Seebeck effect at low temperatures in the nominally paramagnetic insulating state of vanadium dioxide, Appl. Phys. Lett. **121**, 102404 (2022).

[54] W. Xing, R. Cai, K. Moriyama, K. Nara, Y. Yao, W. Qiao, K. Yoshimura, and W. Han, Spin Seebeck effect in quantum magnet $Pb_2V_3O_9$, Appl. Phys. Lett. **120**, 042402 (2022).

[55] K. Oyanagi, S. Takahashi, T. Kikkawa, and E. Saitoh, Mechanism of paramagnetic spin Seebeck effect, Phys. Rev. B **107**, 014423 (2023).

[56] H. Adachi, K. Uchida, E. Saitoh, J. Ohe, S. Takahashi, and S. Maekawa, Gigantic enhancement of spin Seebeck effect by phonon drag, Appl. Phys. Lett. **97**, 252506 (2010).

[57] C. M. Jaworski, J. Yang, S. Mack, D. D. Awschalom, R. C. Myers, and J. P. Heremans, Spin-Seebeck effect: A phonon driven spin distribution, Phys. Rev. Lett. **106**, 186601 (2011).

[58] K. Uchida, H. Adachi, T. An, T. Ota, M. Toda, B. Hillebrands, S. Maekawa, and E. Saitoh, Long-range spin Seebeck effect and acoustic spin pumping, Nat. Mater. **10**, 737 (2011).

[59] T. Kikkawa, K. Shen, B. Flebus, R. A. Duine, K.-i. Uchida, Z. Qiu, G. E. W. Bauer, and E. Saitoh, Magnon polarons in the spin Seebeck effect, Phys. Rev. Lett. **117**, 207203 (2016).

[60] R. Iguchi, K.-i. Uchida, S. Daimon, and E. Saitoh, Concomitant enhancement of the longitudinal spin Seebeck effect and the thermal conductivity in a Pt/YIG/Pt system at low temperatures, Phys. Rev. B **95**, 174401 (2017).

[61] B. Flebus, K. Shen, T. Kikkawa, K.-i. Uchida, Z. Qiu, E. Saitoh, R. A. Duine, and G. E. W. Bauer, Magnon-polaron transport in magnetic insulators, Phys. Rev. B **95**, 144420 (2017).

[62] A. I. Akhiezer, V. G. Bar'yakhtar, and S. V. Peletminskii, *Spin Waves* (North-Holland, Amsterdam, 1968).

[63] A. G. Gurevich and G. A. Melkov, *Magnetization Oscillations and Waves* (CRC, Boca Raton, FL, 1994).

[64] R. M. White, *Quantum Theory of Magnetism*, 3rd ed. (Springer-Verlag, Berlin 2007).

[65] D. D. Stancil and A. Prabhakar, *Spin Waves—Theory and Applications* (Springer, New York, 2009).

[66] S. M. Rezende, *Fundamentals of Magnonics*, Lecture Notes in Physics (Springer, Cham, Switzerland, 2020), Vol. 969.

[67] C. Kittel, Interaction of Spin waves and ultrasonic waves in ferromagnetic crystals, Phys. Rev. **110**, 836 (1958).

[68] J. R. Eshbach, Spin-wave propagation and the magnetoelastic interaction in yttrium iron garnet, J. Appl. Phys. **34**, 1298 (1963).

[69] E. Schlomann and R. I. Joseph, Generation of spin waves in nonuniform magnetic fields. III. Magnetoelastic interaction, J. Appl. Phys. **35**, 2382 (1964).

[70] W. Strauss, Magnetoelastic waves in yttrium iron garnet, J. Appl. Phys. **36**, 118 (1965).

[71] S. M. Rezende and F. R. Morgenthaler, Magnetoelastic waves in time-varying magnetic fields, J. Appl. Phys. **40**, 524 (1969).

[72] M. Weiler, H. Huebl, F. S. Goerg, F. D. Czeschka, R. Gross, and S. T. B. Goennenwein, Spin pumping with coherent elastic waves, Phys. Rev. Lett. **108**, 176601 (2012).

[73] A. Rückriegel, P. Kopietz, D. A. Bozhko, A. A. Serga, and B. Hillebrands, Magnetoelastic modes and lifetime of magnons in thin yttrium iron garnet films, Phys. Rev. B **89**, 184413 (2014).

[74] S. C. Guerreiro and S. M. Rezende, Magnon-phonon interconversion in a dynamically reconfigurable magnetic material, Phys. Rev. B **92**, 214437 (2015).

[75] A. Kamra, H. Keshtgar, P. Yan, and G. E. W. Bauer, Coherent elastic excitation of spin waves, Phys. Rev. B **91**, 104409 (2015).

[76] A. V. Azovtsev and N. A. Pertsev, Magnetization dynamics and spin pumping induced by standing elastic waves, Phys. Rev. B **94**, 184401 (2016).

[77] K. An, K. S. Olsson, A. Weathers, S. Sullivan, X. Chen, X. Li, L. G. Marshall, X. Ma, N. Klimovich, J. Zhou, L. Shi, and X. Li, Magnons and phonons optically driven out of local equilibrium in a magnetic insulator, Phys. Rev. Lett. **117**, 107202 (2016).

[78] D. A. Bozhko, P. Clausen, G. A. Melkov, V. S. L'vov, A. Pomyalov, V. I. Vasyuchka, A. V. Chumak, B. Hillebrands, and A. A. Serga, Bottleneck accumulation of hybrid magnetoelastic bosons, Phys. Rev. Lett. **118**, 237201 (2017).

[79] X. Li, D. Labanowski, S. Salahuddin, and C. S. Lynch, Spin wave generation by surface acoustic waves, J. Appl. Phys. **122**, 043904 (2017).

[80] H. Man, Z. Shi, G. Xu, Y. Xu, X. Chen, S. Sullivan, J. Zhou, K. Xia, J. Shi, and P. Dai, Direct observation of magnon-phonon coupling in yttrium iron garnet, Phys. Rev. B **96**, 100406(R) (2017).

[81] J. Holanda, D. S. Maior, A. Azevedo, and S. M. Rezende, Detecting the phonon spin in magnon-phonon conversion experiments, Nat. Phys. **14**, 500 (2018).

[82] L. Chotorlishvili, X.-G. Wang, Z. Toklikishvili, and J. Berakdar, Thermoelastic enhancement of the magnonic spin Seebeck effect, Phys. Rev. B **97**, 144409 (2018).

[83] S. Streib, H. Keshtgar, and G. E. W. Bauer, Damping of magnetization dynamics by phonon pumping, Phys. Rev. Lett. **121**, 027202 (2018).

[84] K. An, A. N. Litvinenko, R. Kohno, A. A. Fuad, V. V. Naletov, L. Vila, U. Ebels, G. de Loubens, H. Hurdequint, N. Beaulieu, J. Ben Youssef, N. Vukadinovic, G. E. W. Bauer, A. N. Slavin, V. S. Tiberkevich, and O. Klein, Coherent long-range transfer of angular momentum between magnon Kittel modes by phonons, Phys. Rev. B **101**, 060407(R) (2020).

[85] A. Rückriegel and R. A. Duine, Long-range phonon spin transport in ferromagnet–nonmagnetic insulator heterostructures, Phys. Rev. Lett. **124**, 117201 (2020).

[86] C. Zhao, Y. Li, Z. Zhang, M. Vogel, J. E. Pearson, J. Wang, W. Zhang, V. Novosad, Q. Liu, and A. Hoffmann, Phonon transport controlled by ferromagnetic resonance, Phys. Rev. Appl. **13**, 054032 (2020).

[87] J. Puebla, M. Xu, B. Rana, K. Yamamoto, S. Maekawa, and Y. Otani, Acoustic ferromagnetic resonance and spin pumping induced by surface acoustic waves, J. Phys. D: Appl. Phys. **53**, 264002 (2020).

[88] J. Holanda, D. S. Maior, O. Alves Santos, A. Azevedo, and S. M. Rezende, Evidence of phonon pumping by magnonic spin currents, Appl. Phys. Lett. **118**, 022409 (2021).

[89] P. Jiménez-Cavero, I. Lucas, D. Bugallo, C. López-Bueno, R. Ramos, P. A. Algarabel, M. R. Ibarra, F. Rivadulla, and L. Morellón, Quantification of the interfacial and bulk contributions to the longitudinal spin Seebeck effect, Appl. Phys. Lett. **118**, 092404 (2021).

[90] E. Saitoh, M. Ueda, H. Miyajima, and G. Tatara, Conversion of spin current into charge current at room temperature: Inverse spin-Hall effect, Appl. Phys. Lett. **88**, 182509 (2006).

[91] A. Hoffmann, Spin Hall effects in metals, IEEE Trans. Magn. **49**, 5172 (2013).

[92] J. Sinova, S. O. Valenzuela, J. Wunderlich, C. H. Back, and T. Jungwirth, Spin Hall effects, Rev. Mod. Phys. **87**, 1213 (2015).

[93] S. M. Rezende, R. L. Rodríguez-Suárez, J. C. Lopez Ortiz, and A. Azevedo, Thermal properties of magnons and the spin Seebeck effect in yttrium iron garnet/normal metal hybrid structures, Phys. Rev. B **89**, 134406 (2014).

[94] F. Reif, *Fundamentals of Statistical and Thermal Physics* (McGraw-Hill, New York, 2008).

[95] Y. Tserkovnyak, A. Brataas, G. E. W. Bauer, and B. I. Halperin, Nonlocal magnetization dynamics in ferromagnetic heterostructures, Rev. Mod. Phys. **77**, 1375 (2005).

[96] A. J. Princep, R. A. Ewings, S. Ward, S. Tóth, C. Dubs, D. Prabhakaran, and A. T. Boothroyd, The full magnon spectrum of yttrium iron garnet, npj Quantum Mater. **2**, 63 (2017).

[97] J. Holanda, O. Alves Santos, R. L. Rodríguez-Suárez, A. Azevedo, and S. M. Rezende, Simultaneous spin pumping and spin Seebeck experiments with thermal control of the magnetic damping in yttrium iron garnet/heavy metal bilayers, Phys. Rev. B **95**, 134432 (2017).

[98] G. D. Mahan, L. Lindsay, and D. A. Broido, The Seebeck coefficient and phonon drag in silicon, J. Appl. Phys. **116**, 245102 (2014).

[99] M. S. Rogalski and S. B. Palmer, *Solid State Physics* (Gordon and Breach Science Publishers, Amsterdam, 2000).